DOE/FG/45960-4
DE- FG02-02ER45960
Oklahoma State University, Stillwater, OK
Technical Report: Final project report for Terahertz Spectroscopy of Complex Matter

Keywords: THz, terahertz, complex matter, spectroscopy, thin films, waveguides, interferometry, ultrafast, time domain

Abstract
This project designed characterization techniques for thin films of complex matter and other materials in the terahertz spectral region extending from approximately 100 GHz to 4000 GHz (4 THz) midway between radio waves and light. THz has traditionally been a difficult region of the spectrum in which to conduct spectroscopic measurements. The "THz gap" arises from the nature of the sources and detectors used in spectroscopy both at the optical (high frequency) side and electronic (low frequency) side of the gap. To deal with the extremely rapid oscillations of the electric field in this frequency region this research project adapted techniques from both the electronics and optics technologies by fabricating microscopic antennas and driving them with short optical pulses. This research technique creates nearly single cycle pulses with extremely broad spectral bandwidth that are able to cover the THz spectral range with a single measurement.

The technique of THz time domain spectroscopy (THz-TDS) has seen increasing use and acceptance in laboratories over the past fifteen years. However significant technical challenges remain in order to allow THz-TDS to be applied to measurement of solid materials, particularly thin films and complex matter. This project focused on the development and adaptation of time domain THz measurement techniques to investigate the electronic properties of complex matter in the terahertz frequency region from 25 GHz to beyond 5 THz ($<1 \rightarrow >165$ cm^{-1}). This project pursued multiple tracks in adapting THz Time Domain Spectroscopy (THz-TDS) to measurement of complex matter. The first, and most important, is development of a reliable methods to characterize the complex dielectric constant of thin films with high accuracy when the wavelength of the THz radiation is much longer than the thickness of the film.

We have pursued several techniques for measurement of thin films. The most promising of these are waveguide spectroscopy and THz interferometry. Since THz spectroscopy measures the changes of the transmitted spectra, any noise on the THz signal contributes to measurement errors. The dynamic range—defined as the RMS noise of the THz detector compared to the peak THz signal—of THz spectroscopy using photoconductive antennas is extremely high, typically over 10,000. However the precision with which spectroscopic data can be measured is limited by the noise on the laser source which is typically 0.1% to 1%. For low values of the sample absorbance, $e^{-\alpha d} \cong 1-\alpha d$, and for values of $\alpha d \leq 10^{-2}$ the change in transmission approaches the measurement accuracy. The sample refractive index can be measured with better accuracy since the index causes a temporal shift of the THz pulse by an amount $\Delta\tau \cong nd/c$ and jitter noise is generally much lower than amplitude noise. Time shifts of tens of femtoseconds can generally be resolved so that index-thickness values of $nd > 10^{-3}$ cm can be accurately measured. Waveguide spectroscopy is a way to increase the path length in thin film by several orders of magnitude, and thus have a large interaction length even when the film is much less than a wavelength in thickness. Film thicknesses of 10's of nm have been measured. THz interferometry cancels out many of the noise sources of THz spectroscopy and can thus result in measurements of films of several hundred nm in thickness and is additionally suitable for optical pump, THz probe spectroscopic techniques.

A large amount of additional work was performed in support of the main project direction or to explore promising alternative avenues for research. This report discussed work on the the confinement of low density species for measurement of nanogram or picogram quantities of material. Whispering gallery mode resonators to achieve long path lengths were also investigated as were imaging techniques for sub-wavelength imaging of thin films. The report concludes with a report on investigations of fundamental issues in THz beam propagation and coupling that impact THz spectroscopy and the other spectroscopic techniques developed during this project.

Project Accomplishments- Contributions to Knowledge and Scholarship

1. Jiangquan Zhang and D. Grischkowsky, " Adiabatic Compression of parallel-plate metal waveguides for sensitivity enhancement of waveguide THz time-domain spectroscopy (THz-TDS)" *Applied Physics Letters*, vol. 86, 061109 (2005).
2. M. M. Awad, R. A. Cheville, "Transmission terahertz waveguide-based imaging below the diffraction limit", *Applied Physics Letters*, vol. 86, 221107 (2005)
3. M. T. Reiten and R. A. Cheville, "Effect of spherical aberration and surface waves on propagation of lens-coupled THz pulses", *Optics Letters*, vol. 30, p. 673 (2005)
4. J. A. Small and R. A. Cheville, "Measurement and noise characterization of optically induced index changes using Terahertz interferometry", *Applied Physics Letters*, vol. 84, p. 4328 (2004).
5. R. Alan Cheville, "Perspectives on THz Time Domain Spectroscopy", *Journal of the Optical Society of Korea*, vol. 8, p. 34 (2004),
6. Jiangquan Zhang and D. Grischkowsky, " THz time- domain spectroscopy of sub-monolayer water adsorption in hydrophilic silica aerogel," *Optics Letters*, vol. 29, p. 1031 (2004)
7. Jiangquan Zhang and D. Grischkowsky, " Waveguide THz time-domain spectroscopy of nm water layers," *Optics Letters*, vol. 19, p. 1617 (2004).
8. Jianming Dai, S. Coleman and D. Grischkowsky, " Planar THz Quasioptics," *Applied Physics Letters*, Vol. 85, p. 884 (2004).
9. Jiangquan Zhang and D. Grischkowsky, " Terahertz time-domain spectroscopy study of silica aerogels and adsorbed molecular vapors," J. Phys. Chem. B, vol. 108, p. 18590 (2004).
10. S. Coleman and D. Grischkowsky, " Parallel plate THz transmitter," Applied Physics Letters, vol. 84, p. 654 (2004)
11. Mathew T. Reiten, Stacee A. Harmon, Richard A. Cheville, "THz Beam Propagation Measured Through 3D Amplitude Profile Determination ", *J. Opt. Soc. Am. B*, vol. 20, p. 2215 (2003).
12. S. Krishnamurthy, M. T. Reiten, S. A. Harmon, and R. A. Cheville, "Characterization of thin polymer films using terahertz time-domain interferometry", *Applied Physics Letters*, vol. 79, p. 875 (2001)

Project Accomplishment- Contributions to the Scientific Workforce

Graduate students:

1. Mathew T Reiten, Ph.D. 2006, currently employed in a startup company in Annapolis, MD.
2. Steven Coleman, Ph. D. 2005, employed in industry.
3. John O'Hara, post-doctoral position in Dr. A Taylor's group at LANL
4. Jiangquan Zhang, Ph.D. 2004.
5. Stacee Harmon, M.S. 2005, currently working towards Ph.D. degree
6. Shyla Krishnamurthy, M.S. 2003, employed at NIH.
7. Jay Small, M. S. 2005, currently working for aerospace company in Tulsa, OK.
8. Mohammed Awad, M.S. 2005, currently pursuing Ph.D. overseas.

Undergraduate students:

1. Pauline Pham, BSEE 2005
2. Leslie Hess, BSEE 2006
3. Justin Waits, BSEE 2004
4. John Madison, BSEE 2004
5. Wendy Siemens, BSEE 2004

Report on Findings and Accomplishments

We have undertaken development and adaptation of time domain THz measurement techniques to investigate the electronic properties of complex matter in the terahertz frequency region from 25 GHz to beyond 5 THz (<1 $\rightarrow$ >165 cm^{-1}). The terahertz spectral region that occurs between radio waves and light has great potential for understanding the properties of materials used in electronics and biotechnology. However measuring thin layers or microscopic amounts of such materials—the most technologically useful forms—has been challenging. This project developed techniques to measure the terahertz properties of films with thicknesses of under 100 nm. These techniques—based on interferometry, guided wave propagation, and novel nano-structured materials—open the door for fundamentally new sensor technologies capable of detecting a wide range of chemical or biological agents, or increasing our understanding of complex matter.

The sensitivity of standard THz spectroscopic techniques as a function of sample thickness is shown in Figure 1 below. The measurement resolution of standard THz-TDS has the limitation that sample index-thickness product must be $\alpha d > 2\%$ and/or $(n-1)d > 5\ \mu m$ due to drifts between reference and sample scans. This is due to noise from optical sources coupled on the THz emitter as well as detector noise that limits the accuracy of measurements. The limits of measurement resolution affect the accurate measurement of thin films, measurements of changes in strongly absorptive samples- i.e. polar liquids, and detection of small sample quantities (μg, ng, pg) of samples using time resolved THz techniques.

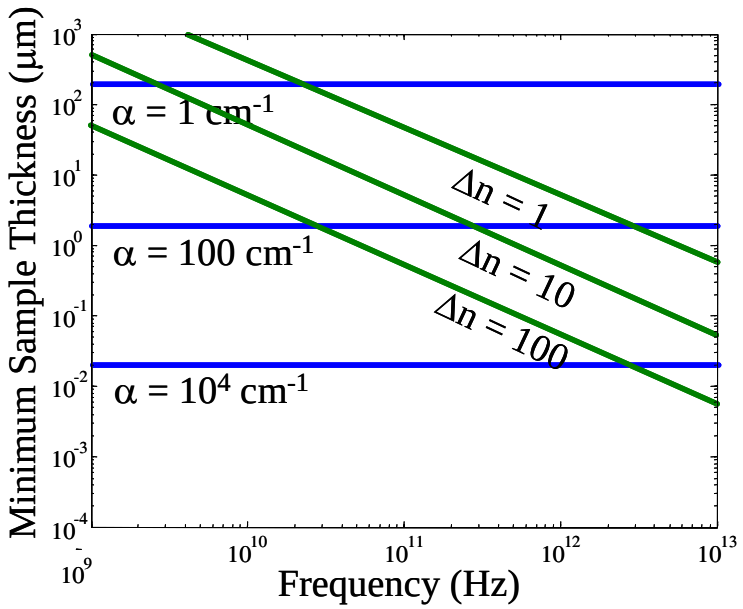

Figure 1: Sensitivity of standard THz time domain spectroscopy as a function of optical thickness (αd) and optical path length (nd).

Waveguide THz Spectroscopy

We have made fundamental progress in development of THz waveguides for spectroscopic measurements. The efficient coupling of broadband THz pulses into waveguides of different configurations is achieved by quasi-optics, which incorporates hyper-spherical or plano-cylindrical silicon lenses. This is a key breakthrough for sensing sub-wavelength thick sample layers in the THz spectral region. For sensitive detection of a thin layer, it is necessary that the interaction region of electromagnetic radiation with the sample material be of the order of a wavelength. Optical wavelengths of several hundred nm have interaction regions of several wavelengths even with relatively thin films. However, for THz wavelengths of several hundred μm, the proportionately sub-wavelength interaction regions result in orders of magnitude less sensitivity for thin films.

Single-mode and low-loss propagation was demonstrated in a plastic ribbon waveguide with pulse broadening due to group velocity dispersion, and in a parallel metal plate waveguide with non-dispersive TEM mode propagation. Planar dielectric waveguides have extensive fringing fields of the propagating THz waves outside the waveguide enabling THz-TDS studies of surface-specific molecular adsorption layers or thin films grown on the waveguide structure. This project also have developed low-loss parallel plate metallic waveguides with extremely low loss and negligible dispersion. These studies have made possible new applications of THz radiation. One of these applications is waveguide THz time-domain spectroscopy (THz-TDS), which can be used to measure the absorption and dielectric constant of a thin nm layer in the waveguide. To enable THz spectroscopy, which compares a sample pulse to a reference pulse, the project investigated in-place layer fabrication and removal techniques for the parallel plate waveguides as shown in Figure 2. Waveguide THz-TDS allows THz spatial confinement to sub-wavelength dimensions together with long propagation lengths, dramatically improving the sample filling factor and consequently the sensitivity. For the TEM mode of parallel plate metal waveguides, the spatial confinement, determined by the separation b between the plates, can be easily λ/10, and one of our goals during this project was to extend this to λ/100 (~300 nm @ 1 THz).

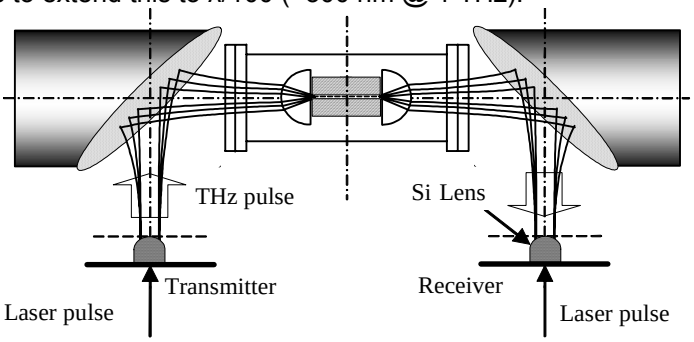

Figure 2: Laboratory detection of 20 nm layers of adsorbed H_2O molecules using THz-TDS.

For the case of a metal waveguide with a thin layer of the substance to be detected, the total loss comes from both the metal walls and the substance layer. By comparing the signal from the empty guide with that from the waveguide containing the layer of material to be detected, the amplitude and phase change caused by the layer can be extracted. Since THz-TDS is a phase sensitive measurement technique, the absorption and index of refraction of the layer material can then be obtained. The sensitivity of this measurement is proportional to the ratio between the length and the plate separation of the waveguide, so that when properly configured, this method can be used to characterize extremely thin layers of low-loss materials. In order to test these predictions and measure the sensitivity of this technique we measured the index and absorption coefficient of adsorbed water. We have demonstrated excellent THz coupling and transmission through the waveguide assembly within the chamber. Using a 63.5 mm long parallel plate waveguide with a plate separation of b = 53 μm, we have characterized bulk water layers of less than 20 nm thickness, equivalent to approximately 64 molecular layers as shown in Figure 3.

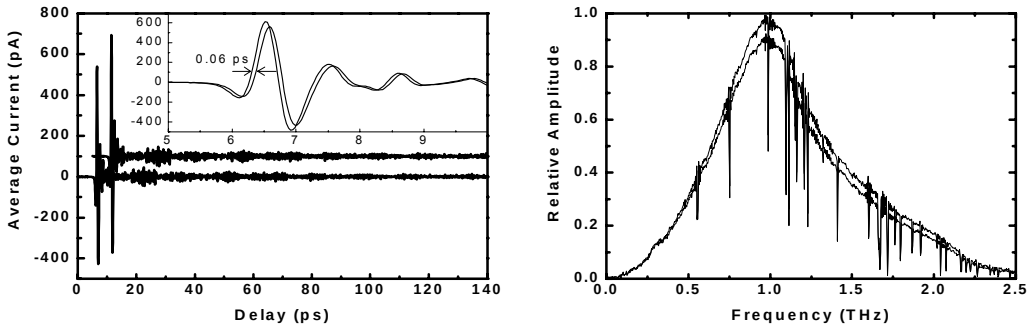

Figure 3: Waveguide THz time-domain spectroscopy of nm water layers. The left figure shows the reference THz pulse (upper trace) and the signal pulse. The two corresponding spectra are shown overlapped on the right.

This project also investigated ways to increase sensitivity of waveguide-based THz sensors by increasing the filling factor, while maintaining the coupling efficiency of THz radiation into these structures. The measurements discussed above and additional measurements done during the project demonstrated relatively good coupling and throughput using a planar waveguide with a plate separation of as small as b = 25 μm, less than λ/10 at 1 THz. Because the measurement sensitivity is proportional to the ratio of sample thickness to b this project undertook a set of experiments to determine the theoretical and practical waveguide spacing—achieving at least 5 μm separation—while maintaining good input and output coupling to the waveguide. However, the coupling efficiency into and out of the waveguide is optimal with b = 150 μm and decreases proportionally with b; b = 50 μm couples 1/3 of the b = 150 μm input signal amplitude. In the case of b < 10 μm very little coupling is expected into the waveguide providing a limitation on the potential sensitivity of waveguide THz spectroscopy.

This project demonstrated a solution to the conflicting requirements of good coupling efficiency together with high sensitivity, as illustrated below. Figure 4 at left shows, on an expanded vertical scale, an "adiabatic" transition from an initial b = 150 μm to a b = 10 μm for the propagation measurement and the exit adiabatic transition to a b = 150 μm for good output coupling. In this case adiabatically means the change in b must take place slowly over a spatial scale of many wavelengths; in agreement with our observations TEM mode propagation is then preserved and there is no reflection. Compared to the water layer measurement with a constant b = 53 μm, the adiabatic guide should in-couple and out-couple more efficiently and be approximately 5 times more sensitive to the layer. By the end of the project period we had constructed a new waveguide assembly which integrates the coupling lenses, adiabatic compressor and waveguide.

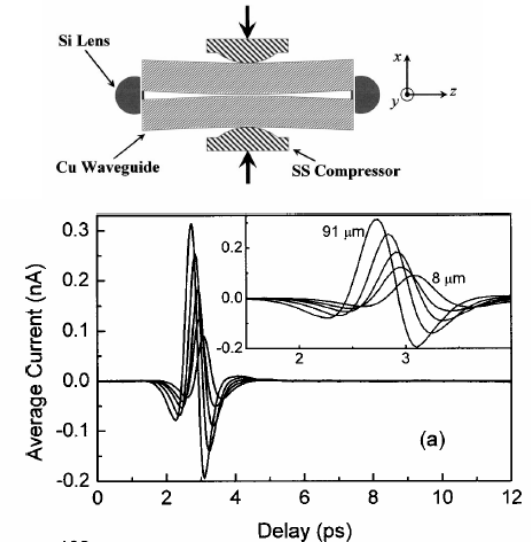

Figure 4: The top figure illustrates the adiabatically compressed waveguide structure. The bottom figure is the output THz pulses from the waveguide with midpoint separations of 91, 48, 24, 12, and 8 μm.

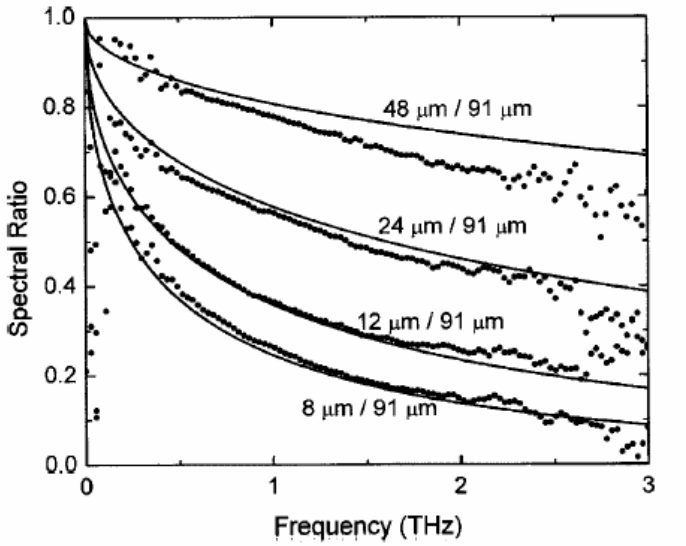

Spectral ratios between the transmitted THz pulses from the adiabatically compressed waveguide and that from the reference guide. The experimental measurements are shown as dots while theoretical predictions are shown as solid lines.

This project developed analytic equations that can be used to compare the amplitude absorption for the reference guide with the adiabatically compressed guide. Since the cylindrical lenses and the plate separation at the ends are fixed, the coupling between the cylindrical lenses and the waveguide is considered to be the same for the reference guide and the compressed guides. The pulse and spectrum changes are solely caused by the different absorption of the compressed guides and the scans from the reference guide are compared with individual scans from the compressed guides. The amplitude spectral ratio gives the relative absorption information and are show in the right part of Figure 4, above. The experimental results and the simple analysis demonstrate and explain the efficient coupling of THz pulses

into and out of an adiabatically compressed parallel-plate metal waveguide. Using this technique, it is possible to achieve both high sensitivity and good coupling to significantly improve the sensitivity of waveguide THz-TDS. Because adiabatic compression does not change the frequency dependence of the absorption coefficient, this technique can determine this dependence with increased sensitivity and accuracy.

Confinement in Nanostructured Materials

In addition to the waveguide measurements this project also attempted confinement and concentration of species to raise the detection limit of species at low concentrations. This set of experiments looked at bulk materials with a high surface area to volume ratio such as silica aerogels or porous silicon. The goal of this approach was to use the extra-ordinary surface area of these materials for detection of high-interest and dangerous materials which may only be present at low concentrations. There is a high surface adsorption on such porous materials which enables highly sensitive THz-TDS characterization. The silica aerogel samples, used in our THz-TDS measurements were specified by the supplier to have a surface area per weight of 800 m^2/g, and a density of 0.092 g/cm^3. Compared with the density of 2.20 g/cm^3 for fused silica, the samples contain approximately 96% free space with a typical pore diameter of ~20 nm and a particle diameter between 2 and 5 nm.

Our THz-TDS characterization of hydrophilic silica aerogels detected sub-monolayers of adsorbed molecular vapors. Aerogel samples were place in a vacuum chamber that could be filled with a variety of gases, including H_2O, D_2O, NH_3, N_2, H_2, CO, CH_3Cl, and CH_3F. The volumetric method was used to measure the gas adsorption in the aerogel, from which concentrations could be obtained to an accuracy of 1%. For the silica aerogel, hydrophilicity is mainly caused by the Si–OH groups, which promotes the adsorption of water and other polar molecules. The amount of water adsorption is directly related to the number of surface hydroxyl groups. Hydrophobicity is achieved by replacing the hydroxyl groups by hydrolytically stable non-polar chemical groups, such as $Si–CH_3$. By heating the hydrophobic aerogel in air at above 200 ºC, the $^{-}CH_3$ groups react with O_2 and transform to ^{-}OH groups, resulting in hydrophilicity in the aerogel. Up to now, the extensive spectroscopy on aerogels has been in the optical and infrared region, while study in the far-infrared (THz) has been neglected.

Using THz-TDS, we characterized dry hydrophilic and hydrophobic silica aerogels. The measured indices of refraction and the power absorption coefficients are presented in Figure 5, below left, where the two indices show marked differences. THz measurements have shown that the Si–OH groups in the hydrophilic sample are responsible for the absorption increase above 1.0 THz. Here, heavy water, D_2O, was used to study the structure of the terminal Si–OH groups in hydrophilic silica aerogel, because the $^{-}$OH groups can be easily replaced by the isotropic ^{-}OD groups by exposing the sample to D_2O vapor; this replacement is reversible by exposing the sample to water vapor. By using THz-TDS to monitor the treatment of hydrophilic silica aerogel with D_2O and H_2O vapor, it was observed that, after the D_2O treatment, the refractive index decreased, indicating a substantial effect by the terminal groups on the silica surface. The power absorption coefficient, however, remained essentially the same below 1 THz for the sample before and after dosing with D_2O. Above 1 THz, the measured absorption was higher for the sample after D_2O treatment than before. This observation showed that the ^{-}OH groups play an important role in the absorption in the frequency range above 1 THz. After re-exposing the sample to H_2O, both the refractive index and power absorption coefficient were almost restored to their original values, indicating that ^{-}OH and ^{-}OD groups are not permanently bound to the aerogel surface.

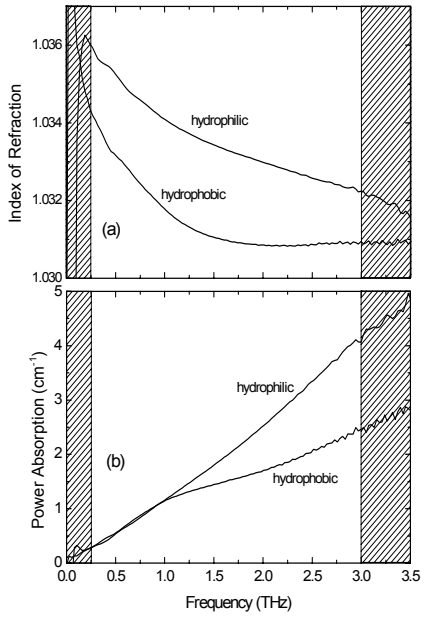

Fig. 5: (a) Indices of refraction and power absorption of hydrophilic and hydrophobic silica aerogels measured as described above.

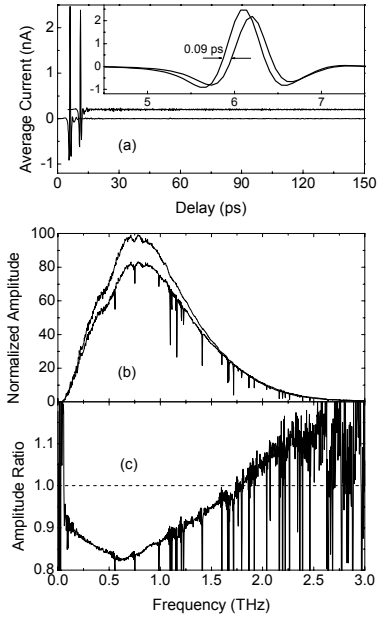

Fig. 6: (a) Output pulses, and (b) spectra of hydrophilic silica aerogel before and after H_2O dosing, and (c) the spectral amplitude ratio. The inset of (a) shows temporal enlargement of the output scans.

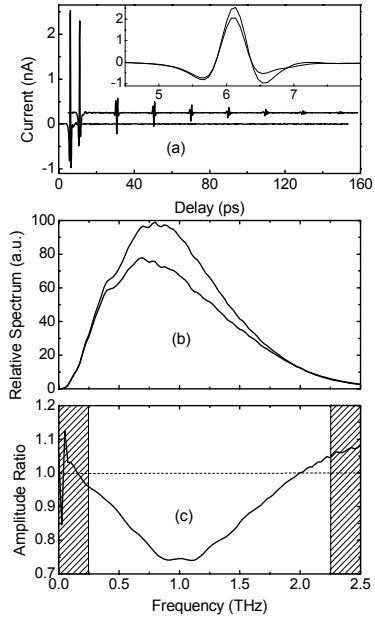

Fig. 7: (a) Output pulses of hydrophilic silica aerogel before and after CH_3F vapor dosing. (b) Spectra for the main pulses in the time range 0-20 ps and (c) the spectral amplitude ratio.

The absorption of THz radiation by adsorbed water is the combinational result of the absorption change due to the OH^- groups being passivated by the adsorbed water, and the increased absorption caused by the adsorbed water itself. At high frequencies, the initial decrease in absorption at low dosing water vapor pressure indicates that the change is dominated by the absorption decrease of the passivated ^-OH groups. As the dosing pressure continues to increase, the observed absorption starts to increase. This observation indicates that the water molecules adsorbed later are not directly bonded to the ^-OH groups, which only serve as absorption centers. As the vapor pressure increases, the following adsorption covers more hydroxyl sites, at the same time water molecule clusters also build up around these sites; these water clusters are believed to be responsible for the broadband absorption increase as the dosing pressure increases. The adsorption only occurs on the surface hydroxyl sites; the portions of silica surfaces without hydroxyl groups are not covered with water molecules even at pressures close to saturation. This understanding has been confirmed by our THz-TDS measurements described below and shown in Figure 6.

This project also used THz-TDS to investigate the adsorption of CH_3F in hydrophilic silica aerogel. The experiment and calculation procedures were similar with that for the adsorption of water vapor and showed that the adsorbed CH_3F was in submonolayer form. Compared with the results of the adsorption of water, the number of adsorbed molecules for CH_3F was approximately one order of magnitude lower, $\Delta N = 2.76 \times 10^{20}$, showing a weaker adsorption of CH_3F by the aerogel sample. Figure 7 presents the transmitted THz pulses through the aerogel sample in vacuum and after the CH_3F adsorption, with the latter shifted for clarity. The respective spectra of the main transmitted pulses in the time range of 0—20 ps are presented in the lower half of the figure along with the corresponding spectral ratio.

The above review of this project's THz-TDS measurements on aerogels documents the promise of these high surface area to volume materials for use in detection of molecular vapors of all types. Clearly, specificity to different vapors has been demonstrated with very large differences in the adsorption

strengths and large differences in the absorption strengths. For example, by THz-TDS we have characterized the surface adsorption of hydrophilic silica of the molecular vapors H_2O, D_2O, NH_3, N_2, H_2, CO, CH_3Cl, and CH_3F. From this list H_2O, D_2O and NH_3 are strongly adsorbed and have similar absorption strengths for THz radiation. CH_3Cl, and CH_3F adsorb almost a factor of 10 more weakly, but their absorption strengths for THz radiation are almost a factor of 10 stronger, so that they are detected with the same efficiency. N_2, H_2, and CO do not adsorb, do not interact with the surface, and do not absorb THz radiation within our instrumental bandwidth.

THz Whispering Gallery Mode Resonators

Whispering gallery modes (WGM) which occur in dielectric spheres and cylinders, describe electromagnetic radiation circulating around the inner surface of optical and microwave cavities. Due to the total internal reflection associated with these modes, they can have cavity Q values exceeding 10^{10} and are being investigated for ultra-narrow linewidth, high-energy density and sensing applications. In addition, WGM cavities are being investigated as frequency selective devices in millimeter and optical wave regions. We are investigating sub-ps THz pulses propagating as a superposition of WGM modes of a dielectric cylinder which is achieved through efficient coupling between a single-mode dielectric slab waveguide and a dielectric cylindrical WGM resonator. The coupled WGM pulse covers a continuous frequency range from 0.4 THz to 1.8 THz and consists of a superposition of several WGM modes. Due to the potentially high Q and low loss of WGM resonators, it may be possible for spheres or cylinders coated with a thin layer of a solid material to be extremely sensitive spectroscopic measurement tools due to the potentially long interaction length arising from multiple internal reflections.

This project developed theoretical modeling of the coupling and propagation of whispering gallery modes in conjunction with our experimental capabilities. These are shown in Figure 8 below. The figure on the left shows WGM pulses that have propagated one time and two times around the circumference of a silicon cylinder respectively. The corresponding spectral oscillations of the cavity pulses are shown in Fig. 3 and indicate the multimode composition of the WGM-THz pulse; the oscillations occur because the phase velocities are different for the individual WGM modes and interference occurs when they are coherently combined at the coupling point. Due to the high dispersion of the whispering gallery modes the necessary interaction lengths for a large number of circumnavigations of the resonator is simply not practical for broad bandwidth THz pulses. However the theoretical understanding gained shows that this technique has potential for narrow bandwidth THz experimental techniques such as backwards wave oscillators or CW photomixing.

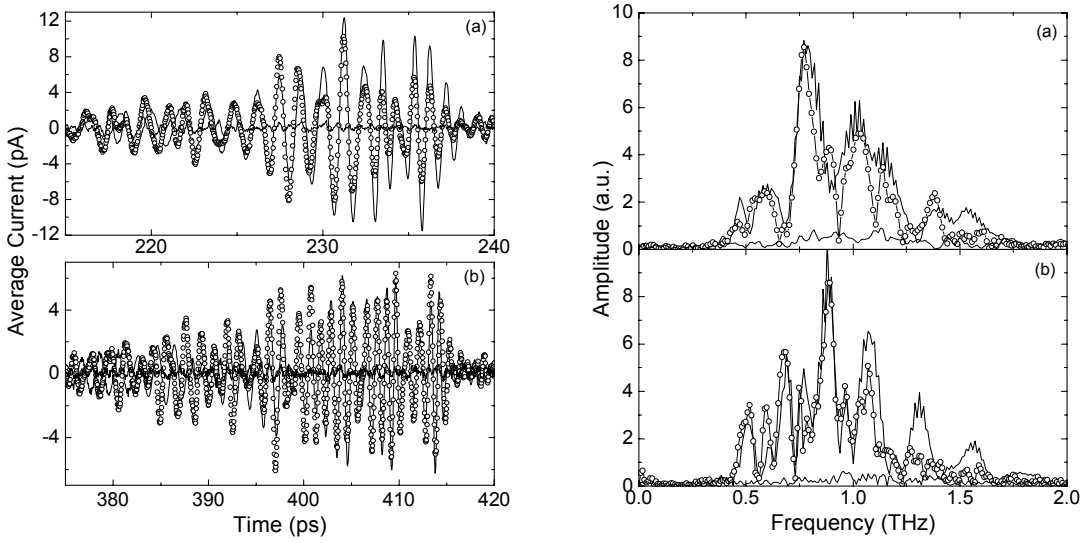

Figure 8: The figure on the left shows the measured and calculated results of (a) the first and (b) the second cavity pulses. The thin solid lines are references, open circles represent the experiment, and the thick solid lines are calculation results. The figure at right is the spectra of (a) the first and (b) the second cavity pulses shown at left. The thin solid lines are references, dotted lines with open circles represent experiment results, and the thick solid lines are calculation results.

THz Interferometry

An alternative technique to measure thin films developed during this project is THz interferometry which splits the THz pulse train into two equal parts, providing a near π, frequency independent phase shift to one of the parts. Such phase shifts are typically obtained by changing the length one arm of an interferometer, however distance changes provide the necessary phase shift only at discrete frequencies which is unsuitable for broad bandwidth THz pulses. In the THz interferometer developed during this project a near π phase shift was achieved through total internal reflection or geometrical rotation of the electric field vector with a roof mirror as shown in Figure 9 below. Phase shifts obtained through total internal reflection approach π only in the limit of incident angle near 90° or an infinite index of refraction. Geometrical field vector rotations are the most effective, however they require the THz beam to have rotational symmetry to achieve a π phase shift. In the THz interferometer destructive interference occurs between two THz pulses which eliminates the background signal, drift, and some noise sources. For the experiments performed this was accomplished via a Michelson interferometer, although a Mach-Zender interferometer was also demonstrated.

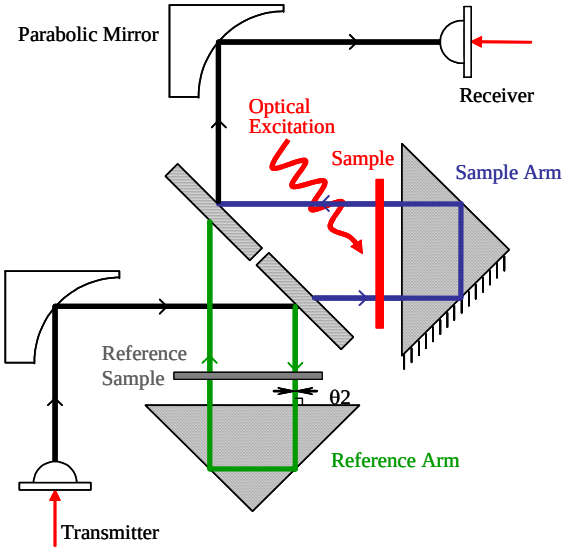

Figure 9: Experimental layout of THz interferometer configured for measuring effect of optical excitation on the complex index in the THz spectral range.

The THz interferometry developed during this project was capable of measuring subwavelength changes in optical path in thin films. This technique is, in effect, phase coherent white light interferometry. The film thickness resolution is less than the Sparrow criterion which states that two pulses are resolvable if there is a minima between their peaks. In measuring the superposition of two pulses of opposite sign, when one pulse is time shifted relative to the other by an amount large enough that the summation of the pulses is above the signal to noise ratio of the system, a signal is measurable. The measurable time shift is determined by the time rate of change of the measured electric field, $\partial/\partial t\ E(t)$ and this is more sensitive for high bandwidth THz signals. For typical interferometer data, the measured electric field has a slope of approximately 200pA/ps. With the minimum detectable signal on the order of 0.2 pA, this corresponds to a time resolution of 1 fs or the ability to detect films of thickness on the order of 100 nm. THz systems with higher bandwidth have correspondingly better sensitivity.

This project demonstrated that THz interferometry is less susceptible to some sources of experimental noise. In THz-TDS the transmission coefficient is determined from the ratio between sample and reference scans with magnitude (modulus) $\rho(\omega)$, and phase term (argument) $\varphi(\omega)$. The real part of the complex refractive index, $n(\omega) = n'(\omega)-in''(\omega)$, is extracted from the argument, $\varphi(\omega)$, and the absorption coefficient from the modulus, $\rho(\omega)$. Errors in the measurement of $n(\omega)$ are proportional to the variance of the modulus. In the case $\rho(\omega)$ approaches unity, the variance is simply proportional to the variance of the noise divided by the spectral amplitude of the reference pulse. Noise contributions arise from three sources which correspond to the THz emitter, shot noise in the THz detector, and other signal independent noise sources such as laser noise, electronic noise, and Johnson noise. The dominant

noise term comes from the THz emitter. For regular THz spectroscopy, the sample and reference scans are measured independently and the noise on the sample and reference scans are uncorrelated. However for THz interferometry, the noise figure is given by the variance of the measured interference signal, and the emitter noise and shot noise contributions are dramatically reduced.

Several demonstrations were performed to characterize the sensitivity of THz interferometers. The first set of tests was on thin, free-standing polymer films of nominally 2 μm thick films of DuPont type C Mylar® polyester film. The measured pulses in the two arms of the interferometer are shown in Figure 10. The nearly 180° phase shift of the one arm relative to the other is clearly seen. The measured signal (points) when a 2 μm thick Mylar® sample is placed in one arm of the interferometer. The small value of $k_o(n-1)d$ makes these two THz pulses nearly indistinguishable. It would be nearly impossible to extract useful data from THz time domain spectroscopy on this sample. The right half of Figure 10 shows the measured interferometer signal with both sample and reference arms open. The measured peak to peak signal here is 3.5% of the difference between the peaks of the reference and sample arms, near the limit of being indistinguishable using normal THz spectroscopic techniques. However, using interferometry the signal change is clearly visible. The experimental results were in good agreement with the estimated index and film thickness. The absorption of the thin polymer film is not measurable since the absorption length $2\alpha L$ is << 1 as shown by the lower line.

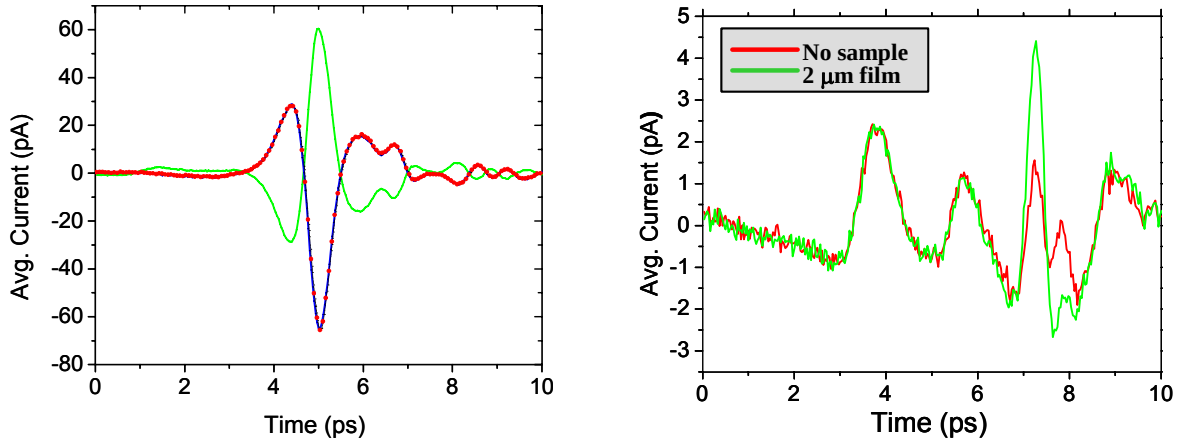

Figure 10: The left figure shows the THz pulses measured in the reference and sample arms of the interferometer shown in Figure 9, the red dots are the measured signal after the polymer film is placed in the sample arm. The right figure shows the change in the interferometer signal with both arms open.

Further refinement of THz interferometry during the project involved demonstrating the sensitivity of measuring optical excitation in semiconductor materials. In this set of experiments the index of refraction of a high resistivity, >10 kΩ-cm silicon wafer is modified through optical excitation. To compare measurements to theory the frequency dependent change in refractive index was described by the Drude model which has been shown to be extremely accurate at THz frequencies in many semiconducting materials. Figure 11 compares the difference between two consecutive THz scans taken with and without optical excitation for standard THz time domain spectroscopy and the differential signal from the THz interferometer. This comparison shows the noise improvement of THz interferometry for optically thin samples. These differences are more apparent when extracting the optically induced change in refractive index, $\Delta n(\omega)/n$, obtained from THz interferogram (points) and that determined by THz-TDS (open circles). The index change calculated using Drude theory is shown as a solid line. It can be seen that the technique of THz interferometry developed during this project provides a sensitive tool for characterization of thin films. Index changes of < 10^{-4} can be measured, corresponding to a change in optical path length of ~340 nm for typical semiconductor wafer thicknesses. At 0.7 THz, the peak of the THz amplitude spectrum, this is an optical path length change of λ/1250. Extrapolating the results to a unity signal to noise ratio, the measurement limit of the system is 32 nm or λ/13,500. This technique

lends itself to optical pump – THz probe spectroscopy with extremely high sensitivity, a powerful tool for understanding complex matter.

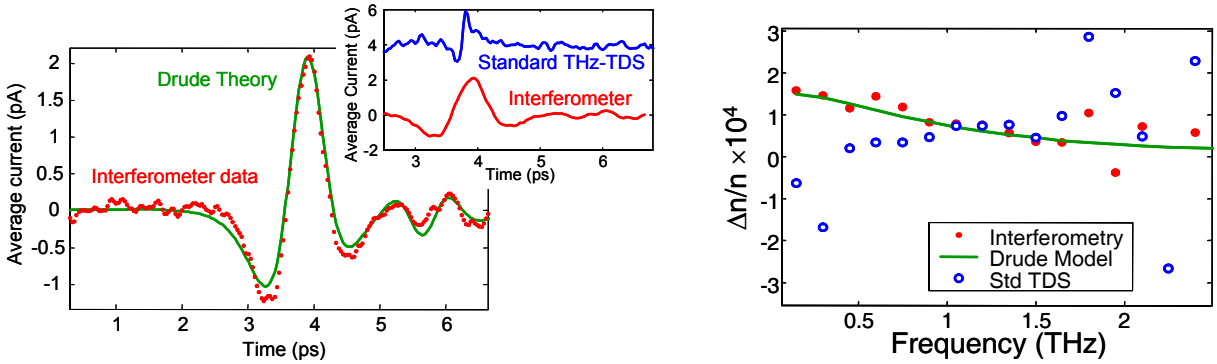

Figure 11: The figure on the left shows THz pulses measured using THz interferometer compared with Drude theory. The inset shows a comparison of the difference between two THz pulses measured using standard THz time domain spectroscopy and the differential pulse from the interferometer. The figure at right shows the optically induced change in refractive index determined from THz interferometry (dots), THz-TDS (open circles), and Drude theory (line).

During this project we have demonstrated THz time domain interferometry can measure photo-induced refractive index change at THz frequencies of $\Delta n/n < 10^{-4}$, and demonstrated sensitivity to changes in optical path length comparable to those previously obtained with differential time domain spectroscopy (DTDS). However unlike DTDS it is straightforward to perform optical pump, THz probe spectroscopy Analysis of noise sources of THz-TDS performed during the project show the measurement sensitivity arises from reduction of both emitter and shot noise and can result in an increase in sensitivity by approximately a factor of 50×.

Imaging Thin Films

In the vein of thin film measurement techniques in this project a technique for subwavelength imaging of thin films was developed based on a modification of tomographic imaging. Although there is currently much interest in developing imaging techniques at terahertz (THz) frequencies, the imaging resolution of all these techniques is limited by the wavelength (sub-mm). To bypass this limit, near field imaging using apertures has been used, but attenuation by the aperture causes the THz radiation to be severely attenuated. Such attenuation is not a factor, however, in the case of propagation through parallel plate waveguides since recent demonstrations have shown the losses are primarily determined by the overlap of the free space THz field pattern and the waveguide mode. At THz frequencies, parallel plate guides can be used as high brightness line apertures with widths substantially less than a wavelength.

In this project the technique of waveguide THz spectroscopy was extended to demonstrate a sub-wavelength line excitation which allows imaging at less than the diffraction limit. This technique has been previously demonstrated at millimeter wave frequencies to achieve spatio-temporal measurements of carrier relaxation. During this project measurements showed it is possible to gain enhancements to resolution by using a line source with image reconstruction done via the Radon transform. To demonstrate THz imaging a 0.4 mm thick silicon wafer with a sub-mm planar horn antenna structure was used as the imaging target. The target was mounted on a rotation stage mounted on a translation stage having resolution of rotational and linear motion of 1° and 10μm, respectively. To create an image a projection set is acquired by moving the translation stage in 20μm increments across the optical axis, resulting in 300 time scans per angle with eighteen projection acquired by varying the projection angle θ from 0° to 170° in 10° increments.

Both confocal cylindrical lenses as well as a waveguide were used to create the line source. Reconstructed images from both confocal cylindrical lens and waveguide imaging setup are shown in Figure 12. To reconstruct the images from line source excitation, time dependent measurements of the THz field were Fourier transformed and a backprojection algorithm was applied to the frequency spectra. The reconstructed images shown correspond to a frequency of 0.6THz for both the cylindrical lens setup

(left) and the waveguide aperture (right) although the data sets have the full bandwidth information of the THz source. Due to the limited number of projection angles acquired, the reconstructed images exhibit line shaped patterns normal to the rotated axis along the s direction that inherent to the backprojection operation. Future improvements to increase the rate of data acquisition will allow reduction of artifacts by acquiring more projection angles is a reasonable time period. The lower portion of the image shows a cross section of the image density function (solid line) and the convolution of the actual image cross-section with a Gaussian of appropriate waist (dashed line). Similar images have been obtained in reflection mode, however considerably more work is required to optimize both forms of THz imaging.

By developing tomographic reconstruction techniques in the THz frequency range, it is possible to obtain images with resolution below the diffraction limit. Future development milestones of this imaging technique are optimization of the number and angle of projections for image reconstruction, developing high-brightness line sources to speed image acquisition, and creating 3D images with subwavelength resolution by time gating the transmitted or reflected signal. As with other imaging techniques, optical excitation beams can be incorporated to add a new dimension for time-resolved measurements.

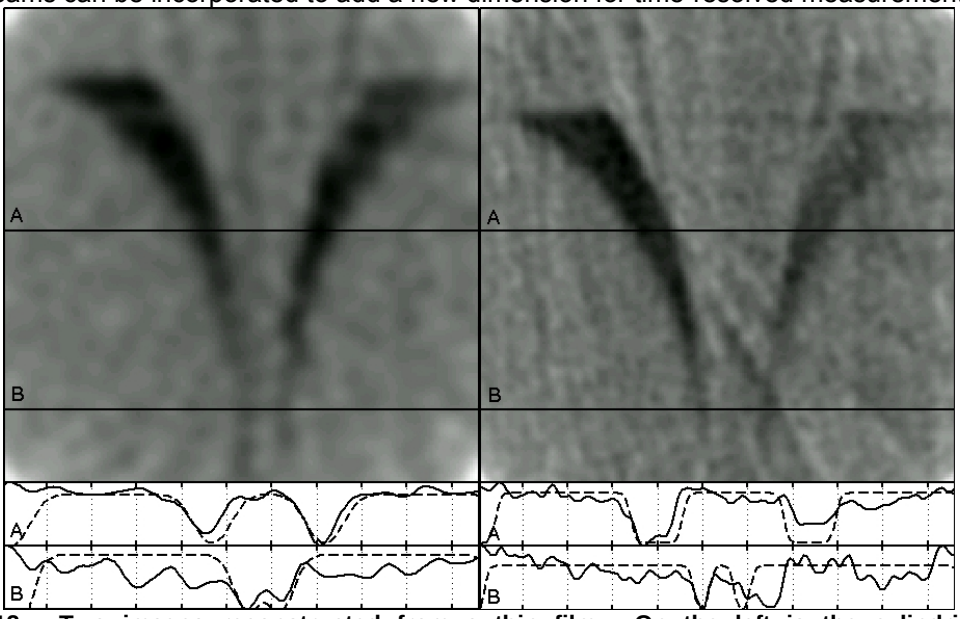

Figure 12: Two images reconstructed from a thin film. On the left is the cylindrical lens reconstructed image and cross section of image density function at A and B. The figure at right shows the waveguide aperture reconstructed image and cross section of image density function at A and B

THz Beam Propagation

The final efforts on this project were done in support of understanding fundamental aspects of THz beam propagation. Since the precise measurement of the time resolved electric field is critical to accurate THz spectroscopic measurements, it is important to understand how beam propagation affects the temporal profile of THz pulses. This is especially true for some of the thin film spectroscopic techniques presented previously. Coupling into waveguides depends very strongly on the overlap integral of the free space THz field with the waveguide mode field. Interferometric techniques require a high degree of rotational symmetry of THz beams in order to achieve good interference and dynamic range. Near single cycle pulses temporally reshape on propagation through free space and temporal reshaping in an optical system can affect the validity of spectroscopic data. The temporal pulse reshaping depends strongly on the spatial profile of the THz beam. Previously reported measurements of the spatial profile of THz beams have found that the THz radiation pattern is adequately represented by a Gaussian with a waist determined by the aperture of the silicon lens used to collimate the THz radiation. This approximation, in the limits within it is valid, permits the ABCD formalism to be applied to determine temporal beam reshaping as well as providing a mathematically tractable approach to calculate the effect of any optical system on a THz beam.

We have extended previous measurements in two dimensions (linear position, time) to three dimensions by measuring the evolution of THz pulses in time on a plane orthogonal to the direction of propagation. Measurements backed by theoretical calculations have correlated spatial profile with beam propagation and experimentally determined the THz beam profile at the THz source silicon lens. Our investigations show that the accuracy of the simple Gaussian beam approach to calculate spatio-temporal evolution of THz beams is not adequate in certain spectroscopic systems. Asymmetries in the beam profile arise from large differences in Fresnel reflection coefficients for different polarization components within the silicon coupling lens, leading to an annular beam profile shown in the top portion of Figure 13. This experimentally measured beam profile is the lens coupled dipole pattern, measured at an image plane. The inset shows the calculated beam profile 1 mm from the lens coupled dipole antenna. This annular structure cannot be well represented by a simple $TEM_{0,0}$ beam profile.

The annular THz beam is best described as a summation of Laguerre-Gauss modes. Hermite-Gauss representations lead to a larger number of modes being required for beam representation. Approximately thirty modes are required to describe the beam. The large number of modes leads to strong beam reshaping which was measured at distances of 16 mm and 116 mm from the THz source. The insets of Figure 13 show calculated beam profiles from code developed during this project. No adjustable fitting parameters were used in prediction of the calculated amplitude profiles. Although not shown similar results are obtained for phase profiles of the THz beam. Using the Laguerre-Gauss basis set to describe beam propagation, we have been able to more accurately predict THz beams propagated through free space and optical systems.

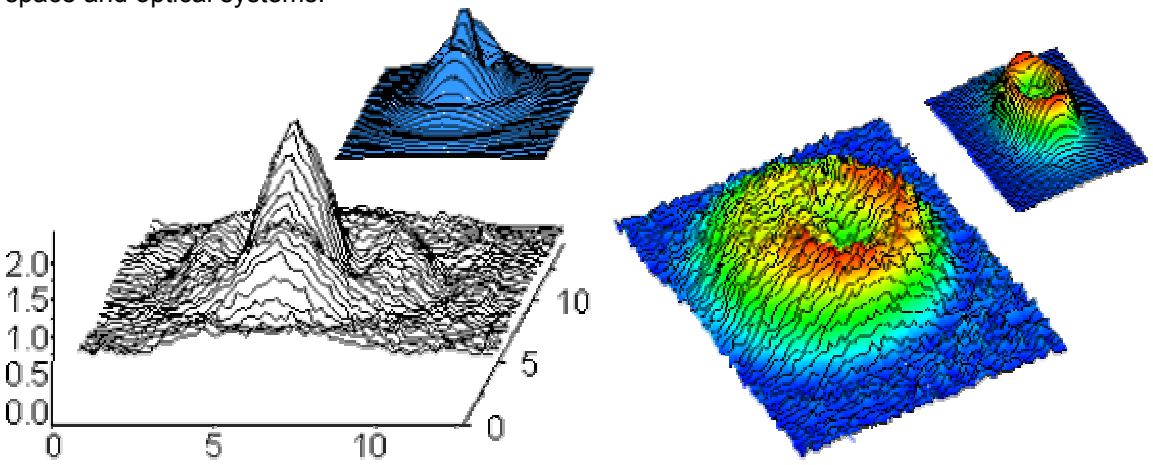

Figure 13: The figure at left shows the measured THz beam profile 16 mm from the THz source. The right figure is the beam profile at an image point in the THz system, for example where the beam would couple to a waveguide. The insets are theoretically calculated beam profiles.

This project also discovered the origins of the Laguerre-Gauss structure of the THz pulse. The annual structure in the frequency domain shown in Figure 13 above results from the inverse analog of the well known pulse reshaping at the focus of a lens. A THz pulse out-coupled from a collimating lens exhibits a universal “swallowtail” shape described by catastrophe theory. This shape results from both spherical aberration and surface waves. The measured swallowtail pulse shape at 16 mm from the THz source is shown in Figure 14, below, and is seen to be a planar pulse front followed by trailing edges or "wings". This shape classified in catastrophe theory as a swallowtail cusp. The spatial amplitude distribution at five discrete frequencies, obtained from a numerical Fourier transform, is shown in the right frame of the figure along with the theoretical prediction based on a simple time-of-flight model based on the stationery phase approximation shown in the inset. In brief, the frequency dependent spatial amplitude distribution results from interference between the time delayed “wings” of the swallowtail and the leading edge. This project also found that some of the swallowtail pulse shape is due to efficient coupling of low frequency components to free space due to surface waves.

The origin of the swallowtail pulse front is thus due both to surface waves and the effect of the lens on the pulse front. A lens in the paraxial limit produces a planar phase front from a diverging spherical wave by

introducing a phase delay proportional to the square of transverse position, (ρ^2). However outside the paraxial limit the pulse front exhibits phase shifts due to third order (Seidel) aberrations. Since the source dipole lies on the optical axis, only spherical aberration contributes, introducing a quartic (ρ^4) phase delay. The swallowtail pulse shape can then be classified using catastrophe theory since the shape results from a polynomial equation, i.e. spherical aberration. Catastrophe theory classifies caustics resulting from a quartic phase correction (ρ^4) as A_3, or axial cusp caustics. Since the phase delay for any ray intersecting a caustic surface at a given point is constant, the shape of the caustic determines the pulse front at any given time and a caustic of a given codimension will generate a pulse front described by the catastrophe of the next highest codimension. Thus, an A_3 spatial caustic (ρ^4 phase delay) will have a pulse front of form A_4 (fifth order polynomial) in time which corresponds to the observed swallowtail pulse.

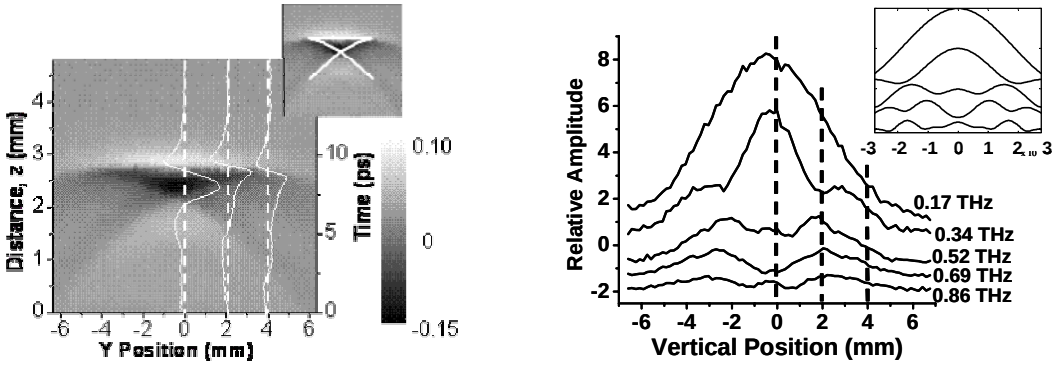

Figure 14: Temporal swallowtail pulse shape measured in the near field region of a THz coupling lens, and the temporal Fourier transform of the field showing the Laguerre-Gauss field structure.

The insights provided by catastrophe theory led to the design of THz free space coupling lenses which create more uniform beam profiles which should lead to increased coupling into THz photonic devices. To improve near field THz beam profiles a lens with an aspheric surface was designed to minimize spatial inhomogeneities due to the interference effects of trailing pulses using the stationary phase model that describes the swallowtail pulses. The lens also maximized the near planar phase front produced by the collimating lens. Two aspheric lens were custom-fabricated from high resistivity silicon. Figure 15 shows the results of the Fourier transform of the measured near-field spatially resolved pulses plotted for fixed frequencies as a function of vertical position. The collimating lens (non-aspheric) spectral profiles demonstrate the previously observed annual structure. The aspheric lens designed during the project gives a more uniform amplitude distribution. A slight experimental misalignment of the collimating lens is evident in the asymmetry of the spectral distributions.

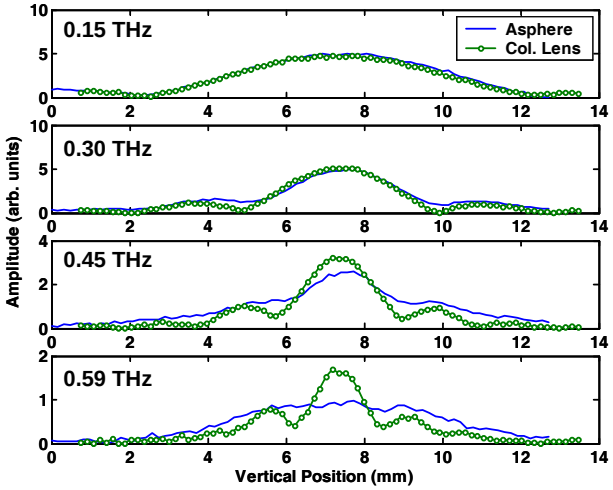

Figure 15: Comparison of silicon aspheric and spherical lenses for coupling THz pulses to free space. The aspheric lens results in considerable field flattening compared with the spherical lens.

The relative contribution of the peak field in the swallowtail pulse has decreased as evident in the unmodulated beam profile measured for the asphere. For the higher frequencies, the measured field for the asphere more directly represents the radiation pattern associated with the small dipole at a dielectric surface. The lower frequencies have a similar spatial distribution for both the collimating lens and the aspheric lens, due to the preferential out coupling of surface waves for long wavelengths as well as possible diffraction effects. A numeric integral taken over the spatial extent of the field amplitude for each Fourier transformed pulse reconstructs the pulse spectra. The spectral overlays have shown that the total field amplitude is the same or less for the collimating lens than the aspheric lens even though the peak field is higher for the on axis component. Additionally the peak response is shifted to lower frequencies compared with the spectral response of a standard TDS system. We are in the process of measuring the effect of aspheric lenses on the THz spectroscopic systems designed during this project.